Dynamically Controllable Two-Dimensional Microvehicle by Coordinated Optical Pulling-Lateral Force

Yuzhi Shi, Hong Luo, Sha Xiong, Tao He, Tongtong Zhu, Qinghua Song, Lei-Ming Zhou, Pin Chieh Wu, Zhanshan Wang, Cheng-Wei Qiu, *Member, IEEE*, and Xinbin Cheng

***Abstract*—Harnessing exotic optical forces promises a plethora of biophysical applications and novel light-matter interactions. The exotic optical pulling force (OPF) and optical lateral force (OLF) have been studied separately, yet synthesizing both candidates simultaneously remains an unsolved challenge and could offer a more powerful manoeuvre of particles. Here, we report a coordinated scheme to harness these two forces together and present a dynamically controlled two-dimensional (2D) microvehicle. The strategy is to leverage unexplored helicity-dependent features of both forces, while the particle size and incident angle of light can also reverse optical forces. The underlying physics of the pulling-lateral force is beyond the dipole approximation, and can be the combined effect from the linear momentum transfer, spin-orbit interactions, etc. Notably, the ratio of both forces can be dynamically and arbitrarily controlled by the ellipticity of incident light solely. The configured 2D microvehicle provides a nontrivial recipe other than using metastructures which require exquisite designs and subtle fabrication processes.**

***Index Terms*—Light polarization, microvehicle, momentum transfer, optical lateral force, optical pulling force, optical tweezers.**

Manuscript received 4 August 2023; revised 25 September 2023; accepted 30 September 2023. Date of publication 16 October 2023; date of current version 23 October 2023. This work was supported in part by the National Natural Science Foundation of China under Grants 61925504, 61905288, 61621001, 62205246, 12104083, 62192770, 62192772, 62020106009, and 62111530053, in part by the Shanghai Pilot Program for Basic Research, Science and Technology Commission of Shanghai Municipality under Grants 17JC1400800, 20JC1414600, 21JC1406100, and 22ZR1432400, in part by the "Shu Guang" Project supported by Shanghai Municipal Education Commission and Shanghai Education under Grant 17SG22, in part by the Hunan Provincial Natural Science Foundation of China under Grant 2020JJ5773, and in part by the Fundamental Research Funds for the Central Universities under Grant DUT22LK27. *(Corresponding authors: Cheng-Wei Qiu; Xinbin Cheng.)*

Yuzhi Shi, Hong Luo, Tao He, Zhanshan Wang, and Xinbin Cheng are with the Institute of Precision Optical Engineering, School of Physics Science and Engineering, Tongji University, Shanghai 200092, China, also with the MOE Key Laboratory of Advanced Micro-Structured Materials, Shanghai 200092, China, also with the Shanghai Institute of Intelligent Science and Technology, Tongji University, Shanghai 200092, China, and also with the Shanghai Frontiers Science Center of Digital Optics, Shanghai 200092, China (e-mail: yzshi@tongji.edu.cn; 2211217@tongji.edu.cn; hetao@tongji.edu.cn; wangzs@tongji.edu.cn; chengxb@tongji.edu.cn).

Sha Xiong is with the School of Automation, Central South University, Changsha 410083, China (e-mail: xiongsha@csu.edu.cn).

Tongtong Zhu is with the School of Physics, Dalian University of Technology, Dalian 116024, China (e-mail: zhutongtong@dlut.edu.cn).

Qinghua Song is with the Tsinghua Shenzhen International Graduate School, Tsinghua University, Shenzhen 518055, China (e-mail: song.qinghua@sz.tsinghua.edu.cn).

Lei-Ming Zhou is with the Department of Optical Engineering, School of Physics, Hefei University of Technology, Hefei 230601, China, and also with the Department of Electrical and Computer Engineering, National University of Singapore, Singapore 117583 (e-mail: zhoulm@hfut.edu.cn).

Pin Chieh Wu is with the Department of Photonics, National Cheng Kung University, Tainan 70101, Taiwan (e-mail: pcwu@gs.ncku.edu.tw).

Cheng-Wei Qiu is with the Department of Electrical and Computer Engineering, National University of Singapore, Singapore 117583 (e-mail: eleqc@nus.edu.sg).

Digital Object Identifier 10.1109/JPHOT.2023.3323623

I. Introduction

HARNESSING optical forces and torques on nano/microparticles show unprecedented advantages in physical and biomedical applications [1], [2], [3], such as quantum levitation [4], [5], DNA folding and stretching [6], [7], bioparticle screening and therapy [8], [9], [10], [11], [12], etc. Though conventional optical forces such as gradient [13], [14], scattering [15], [16] and photophoretic forces [17], [18], [19] have been synergistically utilized for manifold applications, exotic forces such as optical pulling force (OPF) and optical lateral force (OLF) have only been exploited independently due to their normally distinct implementation approaches.

The directions of OPF [20], [21], [22], [23], [24] and OLF [25], [26], [27], [28], [29], [30], [31], [32] are opposite to and perpendicular to the wave vector, respectively. Previously, the OPF has been solely employed with structured light beams such as Bessel beams and other interference patterns [20], [22], [33], [34], [35]. Some composited (e.g., multilayer or core-shell) particles were exploited to enhance OPF and extend the pulling distance [18], [36]. OPFs can also arise from the assistance of the surface plasmon polariton [37], momentum topology [35] or hyperbolic metasurface [21], [38], [39]. By judiciously steering the momentum exchange between a particle and two surrounding media, Kajorndejnukul et al. studied OPF on the particle at an interface [23]. However, the correlation of OPF with light polarization remains unexplored, especially when the previous modelling is based on geometrical optics. We hereby show that this OPF does not necessarily exhibit on particles much larger than the wavelength, and unveil its unexpected tunability with the particle size, the polarization and incident angle of light.

The OLF was recently found on a chiral particle placed above or at an interface by the coupling of chirality and the linearly polarized light [29], also for achiral particles due to spin-orbit interaction inside circularly polarized light beams or interference patterns [27], [40], [41]. The sign of OLF is normally determined

only by the helicity of light, while it could be reversed with the size and chirality of a particle [42], and incident angle of light when the particle size is within the Mie regime [29], [43]. However, the sign reversal effect on an achiral nanoparticle for a fixed helicity was not reported. We will show that, due to the momentum transfer, the OLF can also be reversely subject to the light helicity.

Here, we propose an exquisite scheme to harness these two forces synergically to configure an elegant two-dimensional (2D) microvehicle. Notably, the ratio of two forces is dynamically controlled, covering from negative infinity to positive infinity via only the light ellipticity, namely only by orientating the half-wave plate. Thus, the particle experiencing these two coordinated forces can move in an arbitrary direction. Meanwhile, precisely delivering the particle to a target position facilitates the particle-assembly [44], drug delivering [45], cell targeting [46], etc, which is normally realized by the translation of laser beam in optical trapping [47], or by a purposeful phase profile [48], [49], [50]. Light-powered microvesicles are attracting growing attention because of versatile controls of force and torque, enabling complex manoeuvre of particle. By virtue of recent advances in nanofabrication technology, metastructures can be peeled off from the substrate and move at the interface of air and water illuminated with differently polarized light waves. For instance, translational nano-meta-vehicles are realized by the directional side scattering or spin-orbit interactions [26], [51], [52], [53]. The metastructure can be designed to be self-stabilized when levitated inside a collimated light beam, acting as a promising light sail [54], [55]. Optical torques have also been widely deployed in engineered metastructures to assist more sophisticated trajectories [56], [57], [58], [59]. So far, there lacks a cooperative way to configure a 2D microvehicle that moves in an arbitrary trajectory using optical forces without optical torques. Our subtle 2D microvehicle with coordinated OPF and OLF extends the degree of freedom in the optical manipulation, and inspires new advances in handy and accessible light-powered robots for multifunctional applications in physical and biomedical sciences.

II. Design

We consider a simple scenario that a dielectric spherical particle with a permittivity ε_p is floating at the interface of air ($\varepsilon_{\text{air}} = 1$) and water ($\varepsilon_m = 1.33$), as shown in Fig. 1(a). An obliquely incident linearly polarized plane wave passing through the half-wave plate and the quarter-wave plate becomes an elliptically polarized light beam (wavelength $\lambda = 532$ nm), which is then impinged on the particle. By orientating the half-wave plate with different angles φ, the polarization direction of the linearly polarized light will be altered. After that, the light beam further passing through the quarter-wave plate will become an s, left-hand circular, p, right-hand circular or s polarization, for $\varphi = 0, 45°, 90°, 135°$ or $180°$, respectively. Different polarized light beams will exert optical forces in distinct directions, which can be composed of forces in the x- (F_x, consisting of the optical radiation pressure force and OPF) and y- (F_y, OLFs) directions. Consequently, the particle can move towards four directions

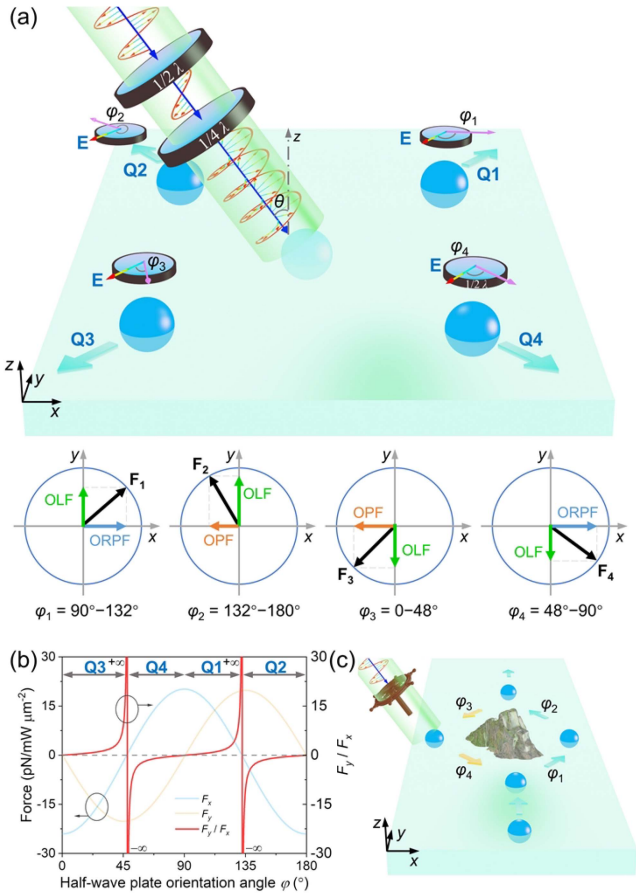

Fig. 1. Synchronization of optical pulling-lateral forces for configuring a simple 2D microvehicle. (a) Schematics of the movement of a particle placed at the interface of air ($n_{\text{air}} = 1$) and water ($n_m = 1.33$) towards an arbitrary direction, which can be realized simply by controlling the polarization of the plane wave, namely by orientating the half-wave plate with an angle φ. The obliquely incident light beam is elliptically polarized with a wavelength $\lambda = 532$ nm and an incident angle θ. The directions of force can be determined by the coordination of the OLF (optical lateral force, F_y), OPF (optical pulling force, negative F_x) and ORPF (optical radiation pressure force, positive F_x). (b) Simulations of F_x, F_y and F_y/F_x with φ. F_x and F_y equal zero at different φ, so that F_y/F_x can be dynamically tuned in a range from negative infinity to positive infinity. Particle radius $a = 750$ nm, $\theta = 24°$, $n_p = 1.45$ (oil). (c) Illustration of the detour of particle by controlling of the orientation angle of the half-wave plate. The particle can move towards the first, second, third and fourth quadrants when $\varphi_1 \approx 90°-132°$, $\varphi_2 \approx 132°-180°$, $\varphi_3 \approx 0-48°$ and $\varphi_4 \approx 48°-90°$, respectively. Thus, by tuning of φ from $0-180°$, the particle can move towards an arbitrary direction.

in four quadrants. This capability relies on the dynamic and continuous control of the optical forces in the x- and y-directions, as shown in Fig. 1(b). F_x and F_y can be zero at different values of φ, causing the ratio of F_y and F_x (F_y/F_x) to transit from negative infinity to positive infinity [red curve in Fig. 1(b)]. By continuously controlling the angle from φ_1 to φ_4, the particle can move along a complex trajectory. For instance, the particle can move along the $+y$-direction when $\varphi \approx 132°$ ($F_x \approx 0$), as shown in Fig. 1(c). When it encounters an obstacle, it can turn to top-right or top-left by setting φ to $90°-132°$ and $132°-180°$, respectively. Remarkably, the moving direction covers angles in $360°$ by orientating φ from $0-180°$.

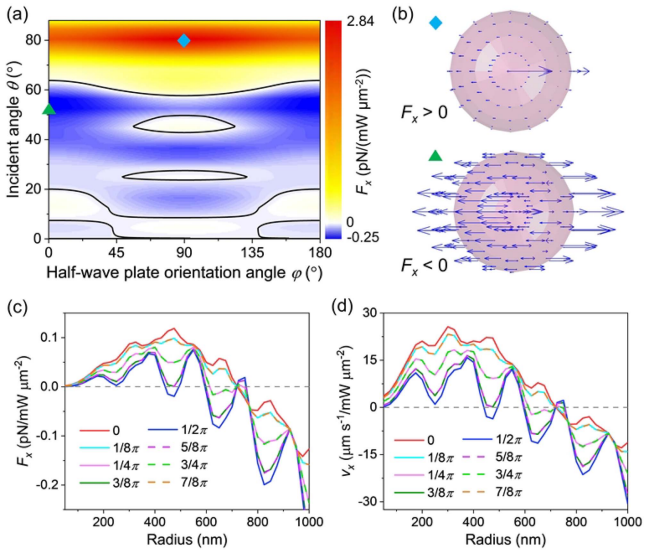

Fig. 2. Anomalous optical pulling forces. (a) Reversible forces in the x-direction, F_x with θ and φ. The OPFs emerge with smaller incident angles of light at certain φ. $a = 750$ nm, $n_p = 1.45$. Black curves represent forces equalling 0. (b) x-y view of force vectors on boundaries (radius = 780 nm) surrounding the particle ($a = 750$ nm). Force vectors are calculated using Minkowski stress tensors. Quadrangle: $\theta = 80°$ and $\varphi = 90°$. Triangle: $\theta = 52°$ and $\varphi = 0$. (c) F_x with particle radius for different polarized light when $\theta = 24°$. Only large particle can generate the OPF by the momentum transfer between air, particle and medium. S polarization ($\varphi = 90°$ or $1/2\pi$) tends to generate OPFs more easily. (d) Particle velocity v_x with radius for different polarized light when $\theta = 24°$.

III. Results

To find an optimal incident angle for F_x and F_y varying between negative and positive values at different φ, so that F_y/F_x can cover a range from negative infinity to positive infinity, we plot the map of F_x with θ and φ, as shown in Fig. 2(a). For incident angles at which F_x does not reverse its sign, such as large incident angles ($\theta > 65°$), they are not suitable for configuring the 2D microvehicle. Thus, $\theta = 24°$ is chosen in Figs. 1(b), 2(b) and (c). The mechanism of negative F_x (OPF) is based on the momentum transfer from air to particle and further to water. Since permittivities of air (ε_{air}), particle (ε_p) and medium (ε_m) satisfy the relationship of $\varepsilon_{\text{air}} < \varepsilon_m < \varepsilon_p$, the photon energy scattered into the medium can be larger than that incident into the particle as predicted by the Minkowski's theory, which describes that the momentum of a photon in a dielectric medium can be given as $p = n\bar{h}\omega/c$, where n is the refractive index of the medium. Consequently, F_x can be negative under a large forward scattering momentum. For instance, the force vectors on a particle when $\theta = 52°$ and $\varphi = 0$ show a dominant net force in the $-x$-direction (OPF), as shown in Fig. 2(b). This linear momentum increase has been demonstrated by floating an oil droplet at the interface of air and water [23], [40]. However, the interpretation of this OPF effect is based on the geometrical optics where the particle radius $a \gg \lambda$. This effect has a strong correlation with the polarizations of light [Fig. 2(a)], as well as the particle size, as shown in Fig. 2(c). Normally, a large radius ($a \geq 600$ nm) is required to induce this OPF, while it has some exceptions when $\varphi = 90°$ ($1/2\pi$, s polarization), showing the emergence of OPF when $a = 450$ nm. The particle can be regarded as a dipole when the radius $a \ll \lambda$, thus only the radiation pressure occurs. Simulations of optical forces in this article are performed in COMSOL using the rigorous Minkowski stress tensor, which is given as [31], [60], [61]:

$$\langle F_{\text{OLF}} \rangle = \oint_S \left\langle \overleftrightarrow{\mathbf{T}} \right\rangle \cdot \hat{\mathbf{n}}\, dA, \tag{1}$$

$$\langle T_{ij} \rangle = \frac{1}{2}\left[D_i E_j^* + B_i H_j^* - \frac{1}{2}\left(\mathbf{D}\cdot\mathbf{E}^* + \mathbf{B}\cdot\mathbf{H}^*\right)\delta_{ij} \right] \tag{2}$$

Here, $\hat{\mathbf{n}}$ is the unit outward normal to the integral surface, and δ_{ij} is Kronecker delta. Simulations are conducted by integrating over the homocentric sphere with a radius 30 nm larger than the particle at the interface. The optical force can be balanced by a fluid drag force expressed as $F_{\text{drag}} = 6f_D\pi\eta a v$, where η is the viscosity of liquid, v is the particle velocity, and f_D is the drag coefficient depending on the viscosity ratio of upper and lower media [62], [63]. By approximately setting $f_D = 0.6$ [62], the particle velocity is calculated [Fig. 2(d)], showing maxium velocities approximately a few tens of microns per second.

To coordinate with F_x and realize a 2D microvehicle, we plot the map of F_y with θ and φ, as shown in Fig. 3(a). $F_y = 0$ when the light beam is linearly polarized ($\varphi = 0$ and 180°, p polarization; $\varphi = 90°$, s polarization). For most incident angles except $11° < \theta < 16°$, $F_y < 0$ and $F_y > 0$ when $0 < \varphi < 90°$ and $90° < \varphi < 180°$, respectively, indicating the correlation of OLF with the helicity of light. The sign of OLF is widely interpreted by the theory of spin-orbit interaction using the dipole approximation, where the particle can be regarded as two dipoles above and beneath water [40].

The equation of a dipole near a surface can be given as $\langle \mathbf{F} \rangle = \frac{1}{2}\text{Re}[\mathbf{p}^* \cdot (\nabla)(\mathbf{E}_0 + \mathbf{E}_D)]$ [55], where $\mathbf{p} = \hat{\alpha}_{\text{eff}}\ \mathbf{E}_0$ is the induced dipole moment near a surface, $\hat{\alpha}_{\text{eff}}$ is the polarizability of particle, $\mathbf{E}_0$ and $\mathbf{E}_D$ are the incident field and re-scattered field by the dipole, respectively. Predicted by the dipole approximation, most OLFs coincides well with the helicity of light. The unexpected sign reversal could be attributed to the momentum transfer between air, particle and water as also indicated in Fig. 2(a) for the sign reversal of F_x in an overlapped range of incident angle (11°–16°). The emergence of OLF can be visualized in Fig. 3(b), where the far-field energies are scattered dominantly to the $+y$- and $-y$-directions for $\varphi = 45°$ and 135°, indicating the negative and positive OLFs, respectively. Compared with F_x, the sign of F_y is more sensitive to particle radius as shown in Fig. 3(c). F_y remains negative for small particles, e.g., $a < 200$ nm, when $0 < \varphi < 90°$, as implied by the dipole theory. It then oscillates around the axis of $F_y = 0$ for some larger particles and eventually has the sign remaining unchanged for even larger particles. The sign of F_y can be easily tuned between negative and positive by orientating the angle φ.

Fig. 4(a)–(d) show F_x and F_y with the relationship of permittivities of particle and medium. For a fixed medium, e.g., water with $\varepsilon_m = 1.33^2$, smaller ε_p facilitates the generation of negative

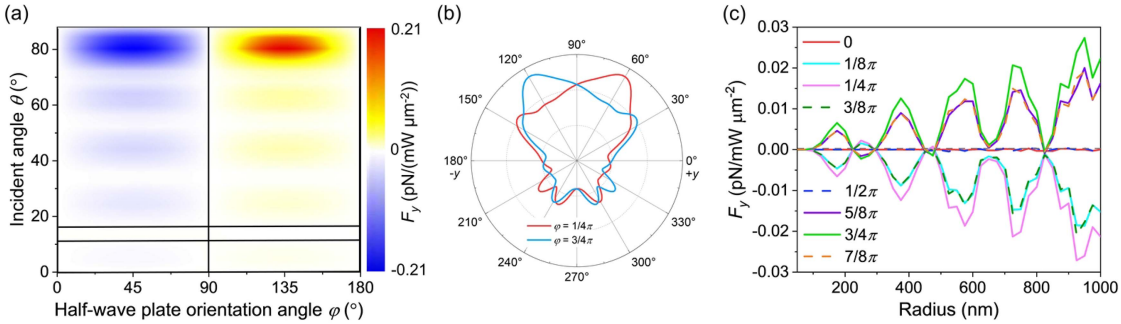

Fig. 3. Anomalous optical lateral forces. (a) Reversible OLFs, F_y with θ and φ. Most F_y remain negative and positive on the left and right sides of $\varphi = 90°$, respectively, coinciding with the consequences of spin-orbit interaction. The exceptions happen when $11° < \theta < 16°$, which may arise from the momentum transfer between the air, particle and medium similar to the mechanism to induce the OPF in Fig. 2(a). $a = 750$ nm, $n_p = 1.45$. (b) Polar plot for the far-field scattering. The far-field light scatters dominantly to the $+y$- and $-y$-directions for $\varphi = 45°$ and 135°, indicating the negative and positive OLFs, respectively. $a = 750$ nm, $n_p = 1.45$, $\theta = 80°$. (c) OLFs with particle radius for different polarized light. The OLFs oscillate with the increment of particle radius. The oscillation could induce the reversal of sign for smaller particles, e.g., $a < 300$ nm. $n_p = 1.45$, $\theta = 24°$.

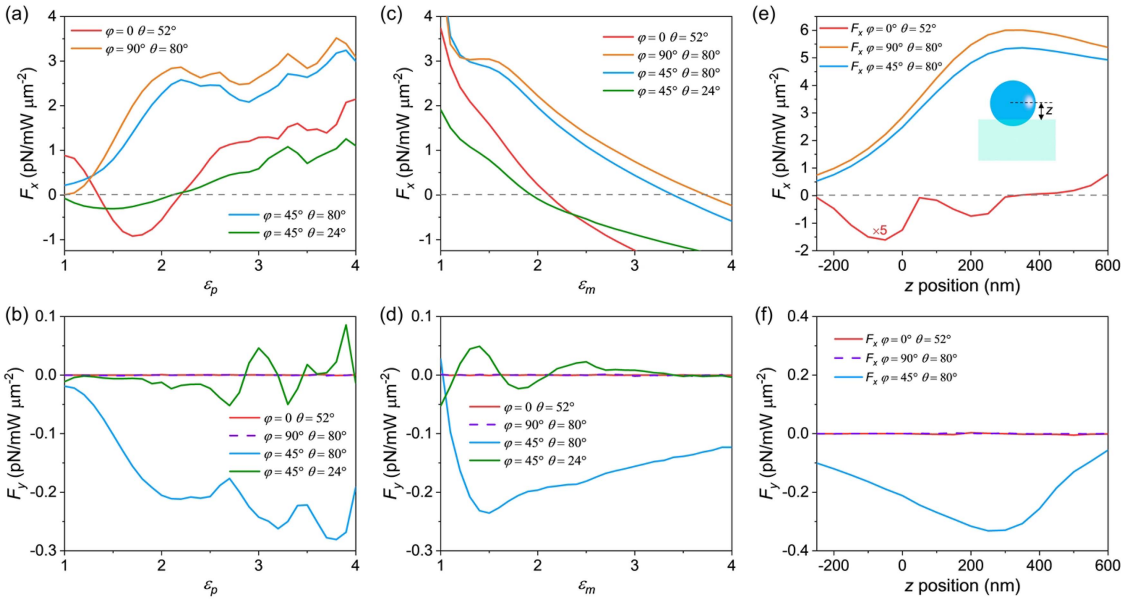

Fig. 4. Optical pulling forces and lateral forces under different parameters. (a) F_x with permittivity of particle ε_p for various θ and φ. The OPF can only occur when ε_p is small, e.g., $\varepsilon_p < 2.2$. (b) F_y with permittivity of particle ε_p for various θ and φ. The oscillation of F_y with ε_p will reverse the sign of F_y when the magnitude of F_y is small for $\theta = 45°$ and $\varphi = 24°$. In (c) and (f), $\varepsilon_m = 1.33^2$. (c) F_x with permittivity of medium ε_m for various θ and φ. Larger ε_m can induce the OPF more easily. (d) F_y with permittivity of medium ε_m for various θ and φ. The large ε_m (e.g., $\varepsilon_m > 1.5$) tends to decrease F_y. In (c) and (f), $\varepsilon_p = 1.45^2$. (e) F_x with the position of particle z. The large z will diminish the OPF by weakening the momentum transfer effect at the interface. $\times 5$ means the data is multiplied by 5. (f) F_y with the position of particle z. F_y increases and then decreases with the increment of z. In (a)−(f), $a = 750$ nm.

F_x for some specific θ and φ. In contrast, larger ε_m is beneficial to the negative F_x [Fig. 4(c)], which can be comprehended by the Minknowski's theory: $p_m = n_m \bar{\hbar}\omega/c$ [64], implying a larger momentum scattered from the particle into the medium than that incident into the particle for a larger n_m. Larger ε_p also induces a strong oscillation on the OLF, which will cause the reversal of sign when the overall magnitude of OLF is small, as shown in Fig. 4(b). The OLF increases and then decreases with the increment of ε_m [Fig. 4(d)], thus water ($\varepsilon_m = 1.33^2$) is well suitable for the generation of OLFs. The portion of particle immersed in water can be dynamically tuned with different densities of the medium. For example, by dissolving a certain amount of KCl into water, one can get a relatively large range of density from 1−1.17 g/cm^3 at a temperature of 20°, while the polystyrene particle has a density ∼1.05 g/cm^3. Whereas the refractive index of the solution only has a narrow range of 1.33−1.38. We then model the F_x and F_y with different positions of particle, as shown in Fig. 4(e) and (f), respectively. F_x has a maximum OPF when $z \approx -50$ nm, while F_y increases then decreases with the increment of z. F_x changes sign from negative to positive when z is greater than 400 nm as the interface system is gradually diminished. Since F_x is typically larger than F_y, setting z from 0 to 300 nm should be feasible for configuring the microvehicle. It is noted that metallic particles are not feasible for microvehicles because of high densities and large radiation pressure forces.

IV. Conclusion

In summary, we unveil unexpected phenomena in optical forces by illuminating a single particle with an elliptically polarized light beam. The effect of momentum transfer correlates strongly with the light polarizations and gives rise to the extraordinary OPF. The spin-orbit interactions generate the reversible OLF with different spins, which could also induce unexpected OLFs together with the momentum transfer between different materials. The polarization-dependent optical forces in two orthogonal directions (x- and y- directions) can be coordinated to facilitate configuring a simple 2D microvehicle capable to move towards any direction as the ratio of F_y and F_x ranges from negative infinity to positive infinity.

The sign of OPF shows strong correlations with light polarizations, which is one of the findings and key strategies for the 2D microvehicle. Another strategy is the reversible OLF, which broadens conventional understanding that the OLF on a single achiral particle depends intuitively on the light spin. Though new characteristics of exotic forces depend closely on the incident angle of light and properties of the medium and particle, the tuning of polarization solely is capable of implementing a 2D microvehicle by synchronizing the OPF and OLF. Compared with current design of microvehicle using metastructures, this scheme eases the design, fabrication/synthesis, and potential experimental implementation for transporting microscopic objects. It can also be extended to a larger scale system (e.g., millimetres or centimetres in dimension) using electromagnetic waves with longer wavelengths (e.g., microwave). We believe that our study not only showcases anomalous and coordinated optical pulling-lateral forces on a single sphere with a simple illumination of the plane wave, but also opens up a new paradigm for extending the degree of freedom in optical manipulation, having great potential in exploiting light-matter interactions, and biological applications, such as tumour targeting, optical binding and drug delivery [64], [65].

References

[1] J. Li, B. Esteban-Fernández de Ávila, W. Gao, L. Zhang, and J. Wang, "Micro/nanorobots for biomedicine: Delivery, surgery, sensing, and detoxification," *Sci. Robot.*, vol. 2, no. 4, Mar. 2017, Art. no. eaam6431, doi: 10.1126/scirobotics.aam6431.

[2] Y. Liu, H. Ding, J. Li, X. Lou, M. Yang, and Y. Zheng, "Light-driven single-cell rotational adhesion frequency assay," *Elight*, vol. 2, no. 1, Aug. 2022, Art. no. 13, doi: 10.1186/s43593-022-00020-4.

[3] T. Cao et al., "Fano resonance in asymmetric plasmonic nanostructure: Separation of sub-10 nm enantiomers," *Adv. Opt. Mater.*, vol. 7, no. 3, Feb. 2019, Art. no. 1801172.

[4] J. Gieseler, R. Quidant, C. Dellago, and L. Novotny, "Dynamic relaxation of a levitated nanoparticle from a non-equilibrium steady state," *Nature Nanotechnol.*, vol. 9, no. 5, pp. 358–364, May 2014, doi: 10.1038/nnano.2014.40.

[5] U. Delić et al., "Cooling of a levitated nanoparticle to the motional quantum ground state," *Science*, vol. 367, no. 6480, pp. 892–895, Jan. 2020, doi: 10.1126/science.aba3993.

[6] K. Neupane, A. N. F. Daniel, R. D. Derek, H. Yu, F. Wang, and T. W. Michael, "Direct observation of transition paths during the folding of proteins and nucleic acids," *Science*, vol. 352, no. 6282, pp. 239–242, Apr. 2016, doi: 10.1126/science.aad0637.

[7] M. D. Wang, H. Yin, R. Landick, J. Gelles, and S. M. Block, "Stretching DNA with optical tweezers," *Biophysical J.*, vol. 72, no. 3, pp. 1335–1346, Mar. 1997, doi: 10.1016/S0006-3495(97)78780-0.

[8] Y. Z. Shi et al., "Sculpting nanoparticle dynamics for single-bacteria-level screening and direct binding-efficiency measurement," *Nature Commun.*, vol. 9, no. 1, p. 815, Feb. 2018, doi: 10.1038/s41467-018-03156-5.

[9] Y. Shi et al., "Nanometer-precision linear sorting with synchronized optofluidic dual barriers," *Sci. Adv.*, vol. 4, no. 1, Jan. 2018, Art. no. eaao0773, doi: 10.1126/sciadv.aao0773.

[10] F. Soto, J. Wang, R. Ahmed, and U. Demirci, "Medical micro/nanorobots in precision medicine," *Adv. Sci.*, vol. 7, no. 21, Nov. 2020, Art. no. 2002203, doi: https://doi.org/10.1002/advs.202002203.

[11] Y. Li, X. Liu, and B. Li, "Single-cell biomagnifier for optical nanoscopes and nanotweezers," *Light: Sci. Appl.*, vol. 8, no. 1, Jul. 2019, Art. no. 61, doi: 10.1038/s41377-019-0168-4.

[12] H. Ding et al., "Universal optothermal micro/nanoscale rotors," *Sci. Adv.*, vol. 8, no. 24, Jun. 2022, Art. no. eabn8498, doi: 10.1126/sciadv.abn8498.

[13] A. Ashkin, J. M. Dziedzic, J. E. Bjorkholm, and S. Chu, "Observation of a single-beam gradient force optical trap for dielectric particles," *Opt. Lett.*, vol. 11, no. 5, pp. 288–290, May 1986, doi: 10.1364/OL.11.000288.

[14] V. Ginis, P. Tassin, C. M. Soukoulis, and I. Veretennicoff, "Enhancing optical gradient forces with metamaterials," *Phys. Rev. Lett.*, vol. 110, no. 5, Jan. 2013, Art. no. 057401, doi: 10.1103/PhysRevLett.110.057401.

[15] A. Ashkin, "Acceleration and trapping of particles by radiation pressure," *Phys. Rev. Lett.*, vol. 24, no. 4, pp. 156–159, Jan. 1970, doi: 10.1103/PhysRevLett.24.156.

[16] P. S. Kollipara and Y. Zheng, "Breaking boundaries in optical manipulation: Beyond Nobel-Prize-winning tweezers," *Photon. Insights*, vol. 2, no. 2, pp. C04–C04, Jun. 2023, doi: 10.3788/pi.2023.C04.

[17] J. Lu et al., "Light-induced pulling and pushing by the synergic effect of optical force and photophoretic force," *Phys. Rev. Lett.*, vol. 118, no. 4, Jan. 2017, Art. no. 043601, doi: 10.1103/PhysRevLett.118.043601.

[18] V. Shvedov, A. R. Davoyan, C. Hnatovsky, N. Engheta, and W. Krolikowski, "A long-range polarization-controlled optical tractor beam," *Nature Photon.*, vol. 8, no. 11, pp. 846–850, 2014, doi: 10.1038/nphoton.2014.242.

[19] I. D. Stoev, B. Seelbinder, E. Erben, N. Maghelli, and M. Kreysing, "Highly sensitive force measurements in an optically generated, harmonic hydrodynamic trap," *eLight*, vol. 1, no. 1, pp. 1–9, Dec. 2021, doi: 10.1186/s43593-021-00007-7.

[20] J. Chen, J. Ng, Z. Lin, and C. T. Chan, "Optical pulling force," *Nature Photon.*, vol. 5, no. 9, pp. 531–534, Sep. 2011, doi: 10.1038/nphoton.2011.153.

[21] R. Jin, Y. Xu, Z.-G. Dong, and Y. Liu, "Optical pulling forces enabled by hyperbolic metamaterials," *Nano Lett.*, vol. 21, no. 24, pp. 10431–10437, Oct. 2021, doi: 10.1021/acs.nanolett.1c03772.

[22] H. Li et al., "Optical pulling forces and their applications," *Adv. Opt. Photon.*, vol. 12, no. 2, pp. 288–366, Jun. 2020, doi: 10.1364/AOP.378390.

[23] V. Kajorndejnukul, W. Ding, S. Sukhov, C.-W. Qiu, and A. Dogariu, "Linear momentum increase and negative optical forces at dielectric interface," *Nature Photon.*, vol. 7, no. 10, pp. 787–790, Oct. 2013, doi: 10.1038/nphoton.2013.192.

[24] O. Brzobohatý, V. Karásek, M. Šiler, L. Chvátal, T. Čižmár, and P. Zemánek, "Experimental demonstration of optical transport, sorting and self-arrangement using a 'tractor beam," *Nature Photon.*, vol. 7, no. 2, pp. 123–127, Feb. 2013, doi: 10.1038/nphoton.2012.332.

[25] A. Hayat, J. P. B. Mueller, and F. Capasso, "Lateral chirality-sorting optical forces," *Proc. Nat. Acad. Sci.*, vol. 112, no. 43, pp. 13190–13194, Oct. 2015, doi: 10.1073/pnas.1516704112.

[26] H. Magallanes and E. Brasselet, "Macroscopic direct observation of optical spin-dependent lateral forces and left-handed torques," *Nature Photon.*, vol. 12, no. 8, pp. 461–464, Aug. 2018, doi: 10.1038/s41566-018-0200-x.

[27] F. J. Rodríguez-Fortuño, N. Engheta, A. Martínez, and A. V. Zayats, "Lateral forces on circularly polarizable particles near a surface," *Nature Commun.*, vol. 6, no. 1, Nov. 2015, Art. no. 8799, doi: 10.1038/ncomms9799.

[28] S. B. Wang and C. T. Chan, "Lateral optical force on chiral particles near a surface," *Nature Commun.*, vol. 5, no. 1, Mar. 2014, Art. no. 3307, doi: 10.1038/ncomms4307.

[29] Y. Shi et al., "Chirality-assisted lateral momentum transfer for bidirectional enantioselective separation," *Light: Sci. Appl.*, vol. 9, no. 1, Apr. 2020, Art. no. 62, doi: 10.1038/s41377-020-0293-0.

[30] H. Chen, H. Zheng, W. Lu, S. Liu, J. Ng, and Z. Lin, "Lateral optical force due to the breaking of electric-magnetic symmetry," *Phys. Rev. Lett.*, vol. 125, no. 7, Aug. 2020, Art. no. 073901, doi: 10.1103/PhysRevLett.125.073901.

[31] Y. Shi et al., "Stable optical lateral forces from inhomogeneities of the spin angular momentum," *Sci. Adv.*, vol. 8, no. 48, Dec. 2022, Art. no. eabn2291, doi: 10.1126/sciadv.abn2291.

[32] T. Cao et al., "Controlling lateral fano interference optical force with Au-$Ge_2Sb_2Te_5$ hybrid nanostructure," *Amer. Chem. Soc. Photon.*, vol. 3, no. 10, pp. 1934–1942, Oct. 2016, doi: 10.1021/acsphotonics.6b00448.

[33] A. Novitsky, C.-W. Qiu, and H. Wang, "Single gradientless light beam drags particles as tractor beams," *Phys. Rev. Lett.*, vol. 107, no. 20, Nov. 2011, Art. no. 203601, doi: 10.1103/PhysRevLett.107.203601.

[34] D. Gao et al., "Optical manipulation from the microscale to the nanoscale: Fundamentals, advances and prospects," *Light: Sci. Appl.*, vol. 6, no. 9, Sep. 2017, Art. no. e17039, doi: 10.1038/lsa.2017.39.

[35] H. Li et al., "Momentum-topology-induced optical pulling force," *Phys. Rev. Lett.*, vol. 124, no. 14, Apr. 2020, Art. no. 143901, doi: 10.1103/PhysRevLett.124.143901.

[36] X. Li, J. Chen, Z. Lin, and J. Ng, "Optical pulling at macroscopic distances," *Sci. Adv.*, vol. 5, no. 3, Mar. 2019, Art. no. eaau7814, doi: 10.1126/sciadv.aau7814.

[37] M. I. Petrov, S. V. Sukhov, A. A. Bogdanov, A. S. Shalin, and A. Dogariu, "Surface plasmon polariton assisted optical pulling force," *Laser Photon. Rev.*, vol. 10, no. 1, pp. 116–122, Jan. 2016, doi: 10.1002/lpor.201500173.

[38] A. Ivinskaya et al., "Optomechanical manipulation with hyperbolic metasurfaces," *Amer. Chem. Soc. Photon.*, vol. 5, no. 11, pp. 4371–4377, Nov. 2018, doi: 10.1021/acsphotonics.8b00775.

[39] D. Lee et al., "Hyperbolic metamaterials: Fusing artificial structures to natural 2D materials," *eLight*, vol. 2, pp. 1–23, Jan. 2022, doi: 10.1186/s43593-021-00008-6.

[40] S. Sukhov, V. Kajorndejnukul, R. R. Naraghi, and A. Dogariu, "Dynamic consequences of optical spin–orbit interaction," *Nature Photon.*, vol. 9, no. 12, pp. 809–812, Dec. 2015, doi: 10.1038/nphoton.2015.200.

[41] H. Chen, C. Liang, S. Liu, and Z. Lin, "Chirality sorting using two-wave-interference–induced lateral optical force," *Phys. Rev. A*, vol. 93, no. 5, May 2016, Art. no. 053833, doi: 10.1103/PhysRevA.93.053833.

[42] T. Cao and Y. M. Qiu, "Lateral sorting of chiral nanoparticles using Fano-enhanced chiral force in visible region," *Nanoscale*, vol. 10, no. 2, pp. 566–574, Jan. 2018, doi: 10.1039/c7nr05464e.

[43] T. Zhu et al., "Extraordinary multipole modes and ultra-enhanced optical lateral force by chirality," *Phys. Rev. Lett.*, vol. 125, no. 4, Jul. 2020, Art. no. 043901, doi: 10.1103/PhysRevLett.125.043901.

[44] J. Zhou et al., "Low-temperature optothermal nanotweezers," *Nano Res.*, vol. 16, pp. 7710–7715, Apr. 2023, doi: 10.1007/s12274-023-5659-1.

[45] S. Campuzano, B. Esteban-Fernández de Ávila, P. Yáñez-Sedeño, J. M. Pingarrón, and J. Wang, "Nano/microvehicles for efficient delivery and (bio)sensing at the cellular level," *Chem. Sci.*, vol. 8, no. 10, pp. 6750–6763, Aug. 2017, doi: 10.1039/C7SC02434G.

[46] H. Xin et al., "Optically controlled living micromotors for the manipulation and disruption of biological targets," *Nano Lett.*, vol. 20, no. 10, pp. 7177–7185, Oct. 2020, doi: 10.1021/acs.nanolett.0c02501.

[47] C. Hong, S. Yang, and J. C. Ndukaife, "Stand-off trapping and manipulation of sub-10 nm objects and biomolecules using opto-thermo-electrohydrodynamic tweezers," *Nature Nanotechnol.*, vol. 15, no. 11, pp. 908–913, Nov. 2020, doi: 10.1038/s41565-020-0760-z.

[48] F. Nan and Z. Yan, "Synergy of intensity, phase, and polarization enables versatile optical nanomanipulation," *Nano Lett.*, vol. 20, no. 4, pp. 2778–2783, Apr. 2020, doi: 10.1021/acs.nanolett.0c00443.

[49] F. Nan and Z. Yan, "Creating multifunctional optofluidic potential wells for nanoparticle manipulation," *Nano Lett.*, vol. 18, no. 11, pp. 7400–7406, Nov. 2018, doi: 10.1021/acs.nanolett.8b03844.

[50] J. E. Curtis, B. A. Koss, and D. G. Grier, "Dynamic holographic optical tweezers," *Opt. Commun.*, vol. 207, no. 1-6, pp. 169–175, Jun. 2002, doi: 10.1016/S0030-4018(02)01524-9.

[51] Y. T. Yoshito, P. Albella, M. Rahmani, V. Giannini, A. M. Stefan, and T. Shimura, "Plasmonic linear nanomotor using lateral optical forces," *Sci. Adv.*, vol. 6, no. 45, Nov. 2020, Art. no. eabc3726, doi: 10.1126/sciadv.abc3726.

[52] Y. Shen et al., "THz time-domain characterization of amplifying quantum-cascade metasurface," *Appl. Phys. Lett.*, vol. 119, no. 18, Nov. 2021, Art. no. 181108, doi: 10.1063/5.0067690.

[53] T. Li, "Reversible lateral optical force on phase-gradient metasurfaces for full control of metavehicles," *Opt. Lett.*, vol. 48, no. 2, pp. 255–258, Jan. 2023, doi: 10.1364/OL.478979.

[54] O. Ilic and H. A. Atwater, "Self-stabilizing photonic levitation and propulsion of nanostructured macroscopic objects," *Nature Photon.*, vol. 13, no. 4, pp. 289–295, Apr. 2019, doi: 10.1038/s41566-019-0373-y.

[55] Y. Shi et al., "Optical manipulation with metamaterial structures," *Appl. Phys. Rev.*, vol. 9, no. 3, Aug. 2022, Art. no. 031303, doi: 10.1063/5.0091280.

[56] S. Zhang et al., "The optoelectronic microrobot: A versatile toolbox for micromanipulation," *Proc. Nat. Acad. Sci.*, vol. 116, no. 30, pp. 14823–14828, Jul. 2019, doi: 10.1073/pnas.1903406116.

[57] D. Andrén, D. G. Baranov, S. Jones, G. Volpe, R. Verre, and M. Käll, "Microscopic metavehicles powered and steered by embedded optical metasurfaces," *Nature Nanotechnol.*, vol. 16, no. 9, pp. 970–974, Sep. 2021, doi: 10.1038/s41565-021-00941-0.

[58] X. Wu, R. Ehehalt, G. Razinskas, T. Feichtner, J. Qin, and B. Hecht, "Light-driven microdrones," *Nature Nanotechnol.*, vol. 17, no. 5, pp. 477–484, May 2022, doi: 10.1038/s41565-022-01099-z.

[59] T. Li et al., "Integrating the optical tweezers and spanner onto an individual single-layer metasurface," *Photon. Res.*, vol. 9, no. 6, pp. 1062–1068, Jun. 2021, doi: 10.1364/PRJ.421121.

[60] Y. Shi et al., "Inverse optical torques on dielectric nanoparticles in elliptically polarized light waves," *Phys. Rev. Lett.*, vol. 129, no. 5, Jul. 2022, Art. no. 053902, doi: 10.1103/PhysRevLett.129.053902.

[61] T. Cao, L. B. Mao, D. L. Gao, W. Q. Ding, and C. W. Qiu, "Fano resonant Ge2Sb2Te5 nanoparticles realize switchable lateral optical force," *Nanoscale*, vol. 8, no. 10, pp. 5657–5666, Feb. 2016, doi: 10.1039/c5nr08804f.

[62] P. Singh and D. D. Joseph, "Fluid dynamics of floating particles," *J. Fluid Mechanics*, vol. 530, pp. 31–80, May 2005, doi: 10.1017/S0022112005003575.

[63] A. Minopoli et al., "ISO-FLUCS: Symmetrization of optofluidic manipulations in quasi-isothermal micro-environments," *eLight*, vol. 3, no. 1, Jul. 2023, Art. no. 16, doi: 10.1186/s43593-023-00049-z.

[64] Y. Shi et al., "Advances in light transverse momenta and optical lateral forces," *Adv. Opt. Photon.*, vol. 15, pp. 835–907, Sep. 2023, doi: 10.1364/AOP.489300.

[65] G. Huang et al., "Upconversion nanoparticles for super-resolution quantification of single small extracellular vesicles," *eLight*, vol. 2, Oct. 2022, Art. no. 20, doi: 10.1186/s43593-022-00031-1.